Carson, B., Westbrook, G.K., Musgrave, R.J., and Suess, E. (Eds.), 1995
Proceedings of the Ocean Drilling Program, Scientific Results, Vol. 146 (Pt. 1)

19. LONG-TERM OBSERVATIONS OF PRESSURE AND TEMPERATURE IN HOLE 892B, CASCADIA ACCRETIONARY PRISM[1]

Earl E. Davis,[2] Keir Becker,[3] Kelin Wang,[2] and Bobb Carson[4]

ABSTRACT

Two holes drilled into the Cascadia accretionary prism during Ocean Drilling Program (ODP) Leg 146 were instrumented with borehole seals ("CORKs") for long-term monitoring of temperatures and pressures at in situ conditions. We report the results obtained during submersible data recovery operations at the sites in September, 1993, 9.5 months after the CORK instruments were emplaced. The installation at Hole 889C off Vancouver Island was severely damaged during a deployment made very difficult by poor weather and unstable hole conditions; no useful data were recovered there. In contrast, the installation at Hole 892B in the accretionary prism off Oregon produced excellent thermal and pressure data that provide constraints on the hydrogeology at that site.

Site 892 is located over the hanging wall of a hydrologically active thrust fault that is penetrated at a depth of about 100 m in the 146-m-deep Hole 892B. In addition, there is a well-defined regional bottom-simulating reflector (BSR) whose depth shoals about 8 m to 72 mbsf at the site, presumably because of the thermal effects of fluid flow in the fault zone. Results of numerical modeling demonstrate that the local shoaling of the BSR is consistent with the effects of recent up-dip fluid flow that initiated roughly 400 yr ago at an average flux per meter along strike of 1×10^{-6} m^{3}s^{-1}; steady-state flow is precluded.

Hole 892B was sealed with a pressure gauge and a 10-thermistor chain extending to a depth of 122 mbsf. Temperatures in the CORKed hole define a generally uniform gradient of about 68 mK m^{-1}. At the depth of the regional BSR, this gradient gives a temperature identical to that on seawater-methane-hydrate phase boundary at the equivalent pressure. The gradient is significantly greater than that defined by shipboard temperature measurements made in exploratory holes about 200 m to the southwest. The disagreement can be explained if the exploratory holes intersected fault-controlled zones of fluid upflow at shallower depths than the CORKed hole. The gradient defined by the shipboard measurements may reflect locally diminished heat flow in the footwall of the fault. CORK temperatures also define a distinct thermal anomaly at the depth of the fault zone, which is consistent with results of numerical simulations of a transient fluid flow event. The up-dip fluid flux is constrained to be approximately 6×10^{-5} m^{3}s^{-1}, nearly two orders of magnitude greater than the average rate inferred from the shoaling of the BSR.

Pressures in the sealed hole decayed from an initial ("shut-in") superhydrostatic value of 70 kPa to a low, relatively stable value of 13 kPa within a few months after drilling (lithostatic pressure at 100 mbsf in this hole is about 630 kPa). The initial superhydrostatic value may have been caused by charging of the formation during drilling, although it is more likely that high pressures were present in the fault zone initially and drained after the fault was penetrated, probably to the surrounding formation spanned by the open section of hole where lower fluid pressure may be present. This conclusion is reached by considering the hydraulic transmissivity required to support the high rates of flow inferred from the CORK and BSR data in light of the transmissivity determinations made at both elevated and reduced pressures by Screaton et al. (this volume).

Attenuation and phase of the seafloor tidal loading signal recorded in the sealed hole remained constant throughout the 9-month recording period at 0.5 and 0.3 hrs (~9° phase lead at 12 hr period), respectively. These characteristics are consistent with the presence of approximately 2% free gas in the pore volume of the sediments below the BSR and above the perforated interval, and high fault-zone transmissivity connecting the perforated interval to the zone above containing free gas.

INTRODUCTION

Sites at four locations were occupied during Ocean Drilling Program (ODP) Leg 146 to study the tectonics and fluid-flow regime of the Cascadia accretionary prism (Shipboard Scientific Party, 1994a). At two sites, holes were equipped with sub-seafloor monitoring instrumentation in order to determine the formation pressure and the thermal structure of the sections after drilling disturbances had dissipated, and to monitor any natural variations if present. The CORK (circulation obviation retrofit kit) long-term borehole observatory instrumentation (Davis et al., 1992) includes a hydrologic seal at the seafloor that prevents fluids from passing into or out of the formation via the drill hole. It allows pressure in the hole beneath the seal to equilibrate with that within the formation spanned by the open hole beneath the level of cemented-in casing. Temperatures are determined at a series of 10 thermistors hanging in the hole, and pressure is measured at a gauge just below the seal. Temperatures, pressure, and other parameters are logged at a selectable interval for periods of up to three years. Data can be retrieved by submersible or remotely operated vehicle (ROV) via an underwater-mateable data port at the seafloor installation.

Site 889

The holes selected for long-term monitoring were Holes 889C and 892B (see Fig. 1 for site locations). Site 889 is located well landward of the deformation front off central Vancouver Island, where folding, faulting, and distributed compressional deformation has more than doubled the roughly 2-km-thick sediment section delivered to the Cascadia accretionary prism by the subducting Pacific plate. The primary objective at this site was to characterize the nature of sediment deformation and fluid flow where there is a lack of coherent strati-

[1]Carson, B., Westbrook, G.K., Musgrave, R.J., and Suess, E. (Eds.), 1995. *Proc. ODP, Sci. Results,* 146 (Pt. 1): College Station, TX (Ocean Drilling Program).

[2]Pacific Geoscience Centre, Geological Survey of Canada, P.O.Box 6000, Sidney, British Columbia V8L 4B2, Canada.

[3]Rosenstiel School of Marine and Atmospheric Science, University of Miami, 4600 Rickenbacker Causeway, Miami, FL 33149, U.S.A.

[4]Department of Earth and Environmental Science, Lehigh University, 31 Williams Drive, Bethlehem, PA 18015, U.S.A.

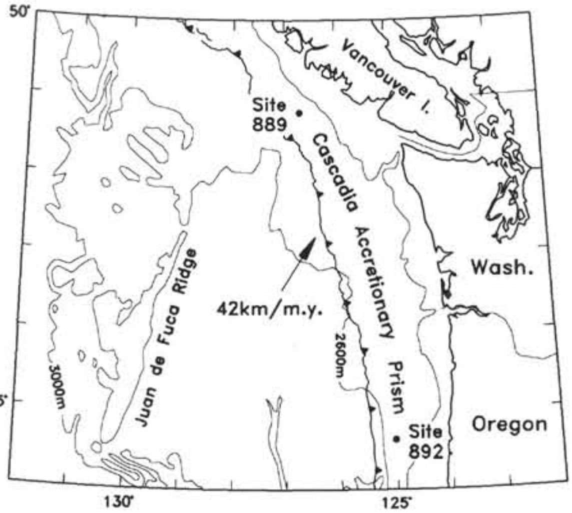

Figure 1. Location of ODP Sites 889 and 892 where borehole instrumentation was deployed.

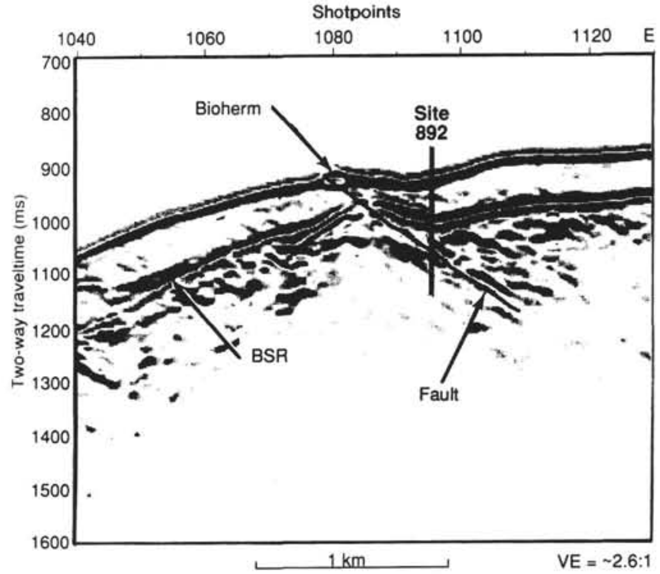

Figure 2. Cross-strike seismic reflection section near Site 892 (Shipboard Scientific Party, 1994c).

graphic reflectors or large-scale deformational structures, but where there is a clearly developed and widespread bottom-simulating reflector (BSR) (Shipboard Scientific Party, 1994b). This locally continuous reflection is believed to be created by the interface between sediments containing solid methane hydrate within the pore volume or other voids, and deeper sediments containing normal pore water and possibly some free gas. CORK observations were intended to refine the estimate of the temperature and pressure at which methane-hydrate is stabilized at this site (see discussion in Hyndman et al., 1992) and to investigate the mechanism of gas hydrate formation within the sediment section (see discussion in Hyndman and Davis, 1992).

Unfortunately, a combination of bad weather and unstable formation created extremely difficult conditions for the CORK installation at Site 889. The thermistor string was damaged during deployment, causing the thermistor leads to be exposed to seawater. As a result, the temperature data are extremely noisy and unreliable. In addition, physical shock during repeated attempts to land the CORK logger appears to have caused the pressure transducer to fail. And, finally, either the CORK seals, or the seal between the casing and formation, appears to have failed. This is inferred from the observation that there was no pressure difference measured across the CORK unit and no tidal pressure attenuation through the formation at the time the site was visited with the submersible *Alvin* roughly 9.5 months after the CORK was installed. Thus, although the data logger was fully functional during the full recording period, all data were compromised (except for internal logger temperature, which remained constant to within 0.2°C, and x-y tilts, which varied by up to 4 mRad over the course of 11 months), and none are presented here.

Site 892

Site 892 was located off central Oregon (Fig. 1), also where the accretionary prism is well developed, local stratigraphic reflectors are incoherent, and a well-defined BSR is present (Shipboard Scientific Party, 1994c). At this site, however, a seismically well-defined thrust fault cuts the section. The fault is imaged to a depth of about 400 m on three adjacent seismic reflection profiles as a discrete reflection that dips landward at an average of 14° (Cochrane et al., 1994).

The site is located over the hanging wall of the thrust fault, roughly 350 m landward of where the fault intersects the seafloor (Fig. 2). The fault lies beneath the site at a depth determined seismically to be 107–113 mbsf (Shipboard Scientific Party, 1994c). The fault is known to be hydrologically active; fluid seepage at the seafloor outcrop of the fault supports biological communities (Moore et al., pers. comm., 1995) and has caused carbonate cements to develop in a 19-km-long zone along strike (Carson et al., 1994). Direct measurements of fluid seepage yield rates locally in a bioherm as high as 2×10^{-5} m^3s^{-1} (Linke et al., 1994). That fluid flow is thermally significant and relatively long-lived is indicated by the local shoaling of the BSR near the position of the fault outcrop. At the position of the Site 892 holes, the seismically imaged BSR lies at a depth of 72 mbsf (Fig. 2; Shipboard Scientific Party, 1994c), slightly shallower than the otherwise constant depth to the BSR, about 80 mbsf, farther from the fault. To the west of the holes, the BSR continues to shoal as the fault outcrop is approached.

Among the objectives of drilling and long-term CORK observations at this site was to sample and monitor conditions in this hydrologically active fault. Also, the site provided another opportunity to investigate the pressure and temperature conditions at the level of the gas-hydrate/free-gas phase transition.

Drilling Observations at Site 892

Five holes were drilled at Site 892 (Fig. 3). All but the shallowest penetrated through the seismically imaged fault and well into the footwall beneath. Holes 892A, 892C, 892D, and 892E, penetrating to depths of 176.5, 176.5, 166.5, and 62.0 mbsf respectively, were drilled within 50 m of one another for purposes of coring, logging, and/or measuring downhole temperatures. Reentry Hole 892B, drilled to a depth of 178.5 mbsf, was located 160 m along strike to the northeast of the closest of the other holes. Although this separation requires any correlations between features identified in the cored, logged, and CORKed holes to be treated with caution, it was felt to be necessary to reduce the possibility of a significant hydraulic interconnection between the non-reentry holes and the CORKed hole. To reduce further the possibility of a hydraulic "short-circuit" and contamination at Hole 892B, each of the non-reentry holes was backfilled with mud and/or cement (Shipboard Scientific Party, 1994c).

Drilling intersected both the BSR horizon and the fault zone, and provided much information about these features and the focused fluid flow at this site (Shipboard Scientific Party, 1994c). Hydrates were

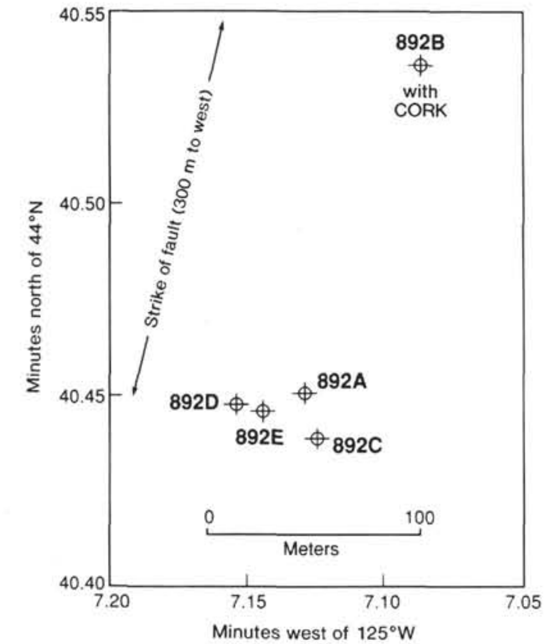

Figure 3. Hole locations at Site 892. The strike of the surface trace of the fault is indicated (from Shipboard Scientific Party, 1994c); the actual position of the trace is well west of the area included in the diagram.

recovered at various levels in the upper parts of the holes, and the presence of free gas in Hole 892C was inferred from vertical seismic profile (VSP) data below the level of the BSR and from the velocity-log data in the section from 72 mbsf to the final depth of the logging run at 130 mbsf. Substantial deformation of the sediment was indicated at numerous levels by high degrees of consolidation and by scaley, sheared, and mélange fabrics. Faults were defined by biostratigraphic reversals, fracturing, and zones of anomalously high porosity. That some of the fractures or fracture zones were currently or recently hydrologically active was indicated by the presence of thermogenic and unstable hydrocarbons, in particular at 68 and just over 100 mbsf, and by locally high temperatures measured with the water sampler and temperature probe (WSTP; Foucher et al., this volume).

SUMMARY OF INSTRUMENTATION AND OBSERVATIONS

Hole Configuration and CORK Instrumentation

Drilling at Hole 892B began with the jetting-in of a 21.6-m length of 16-in conductor casing with the reentry cone and mud skirt. A 14¾-in hole was then drilled to 105 mbsf, and a 93.6-m length of standard 11¾-in casing was hung in the conductor casing and cemented in place. After the cement had set, the cement plug was drilled out and the hole was deepened to the total depth of 178.5 mbsf with a 9 7/8 in. bit. A final section of perforated casing was made up to hang below the cemented section of casing. This extends to 146 mbsf, with the perforated section spanning from 93.4 to 145.6 mbsf. Following the installation of the casing, packer experiments were completed, followed by a final deviation survey during which it was determined that fill had accumulated in the bottom of the hole to a depth of 137 mbsf. The hole was then sealed and instrumented with a CORK observatory system on 15 November, 1992. A summary of the sequence of operations is provided in Table 1.

The thermistor cable deployed in Hole 892B was originally intended for deployment in a deeper hole at Site 891. That site was abandoned as a CORK site when operational difficulties prevented grouting of an exploratory hole. The shallower depth of Hole 892B required the cable to be shortened by folding. The deepest thermistor was positioned at a conservative depth of 122 m to avoid any problems with fill. The final distribution of thermistors with respect to the seafloor, folds, casing segments, and known fill is shown in Figure 4.

Table 1. Hole 892B CORK Operations Summary (all times in UTC).

Hole drilled to 105 mbsf, and 11¾" installed and cemented	92-11-10, 1730 to 92-11-11, 1330
Hole deepened to total depth, and perforated casing set (circulation intermittent throughout)	92-11-13, 1400 to 92-11-13, 2100
Packer pumping tests	92-11-14, 0800 to 92-11-14, 2045
CORK latched in	92-11-15, 1315
First *Alvin* data recovery operations and pump tests, valve left open at end	93-08-31, 1700 to 93-10-04, 0000
Second *Alvin* data recovery operations and valve re-closure	94-08-09, 2000

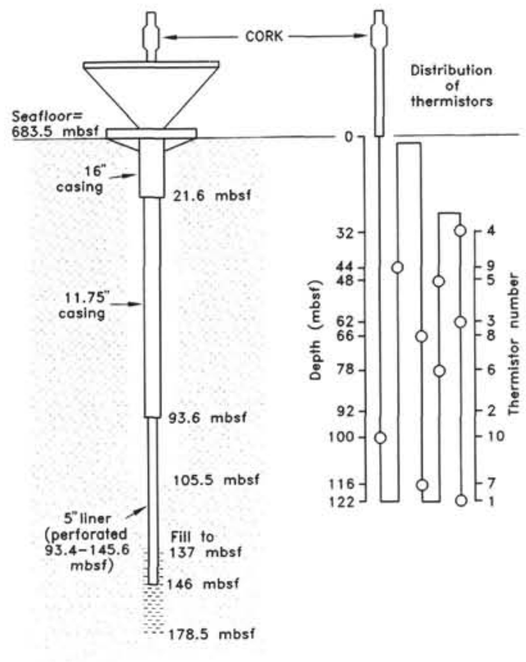

Figure 4. Schematic diagram of instrumented Hole 892B.

Data Recovery Operations

Site 892 has been visited twice with the deep submergence vehicle *Alvin* (Table 1). The first visit, which included several dives in September and October, 1993, allowed a normal data recovery (which provided the primary results described herein), a test of an acoustic link designed to permit two-way communications with the CORK logger from a surface ship (R. Meldrum et al., unpubl. data), and an experiment that involved opening the fluid sampling port to vent fluid from the hole while monitoring the rate of flow and the borehole pressure (E. Screaton et al., unpubl. data). At the end of that series of dives, the fluid sampling port was left open so the hole could vent and formation fluids could be sampled. A second visit with *Alvin* in August, 1994, provided another opportunity to recover data, and to close the fluid sampling port and monitor the early part of the recovery of pressure. Details of this last experiment and of the second and third years of data will be reported at a later date.

Summary of Observations

Temperature and pressure observations for the first 9.5 months of recording are shown in Figures 5 and 6. Over most of the depth of the hole occupied by the thermistor cable, temperatures in the hole were initially warm, up about 2 K in the uppermost part of the hole. Deeper in the hole the formation had been cooled by circulation during drilling, and temperatures warmed through time toward steady values. Equilibration times varied somewhat between thermistors, but most of the drilling-induced transients dissipated within a few weeks after the CORK was latched in. Thermistor 9 at 44 mbsf behaved in an "ideal" manner, decaying to a stable value after about 3 months. Others showed small long-term variations that persisted over the entire recording period. Thus, some caution must be used in accepting the "equilibrium" values shown in Figures 5 and 7. Uncertainties could exceed 0.5°C.

By far the most unusual behavior is exhibited by thermistor 10 at 100 mbsf. Temperature stabilized at this level rapidly after shut-in, but then began to rise roughly 4 months later. By the end of the first recording period 5.5 months after the onset of the transient, the temperature had risen 4°C above that observed during the initial period of stability.

The history of pressure (Fig. 6) reveals several notable features. Pressure in the hole at the time the CORK was latched in climbed immediately to a level roughly 70 kPa above hydrostatic, then decayed toward a fairly steady value averaging 13 kPa above hydrostatic 5.5 months after shut-in. Superimposed on the long-term variation is a tidal signal which is well correlated with that estimated at the seafloor, but obviously attenuated.

Tilt behaved in a manner similar to that in Hole 889C for the first 9.5 month recording period. The system generally stabilized over the first week after installation, then varied by up to about 4 mRad over the remainder of the period. Variations were substantially less over the next ten-month period, although tilts continued to change by about 0.8 mRad. Deflection from vertical of both instruments (Holes 889C and 892B) was about 2 degrees.

THERMAL STRUCTURE

Geothermal Gradient and Heat Flow

Equilibrium temperatures estimated for the formation (Fig. 5) are plotted against depth in Figure 7, along with WSTP measurements made during drilling in Holes 892A, 892D, and 892E, and the position of a few of the most relevant features of the holes and surrounding formation. Ignoring the seafloor temperature, the WSTP data define a gradient of 51 mK m^{-1}. Using an average conductivity for the section of 1.04 W m K^{-1} derived from measurements in cores, a heat flow of 53 mW m^{-2} was determined by the Shipboard Scientific Party (1994c). Two anomalously warm temperatures at 67.5 and 87.5 mbsf fell above this trend by 1.6° and 2.5°C, respectively. The CORK data, including the seafloor temperature point, and excluding only the temperature at 66 mbsf, define a considerably higher gradient of 68 mK m^{-1} and a heat flow of 71 mW m^{-2}. It could be argued that the difference in heat flow is real, and is the consequence of the non-coincident locations of the holes (Fig. 3). Significant local heat-flow variations are likely to exist both across the hanging wall (see results of the modelling discussed below), and along strike (as a result of local variations in the hydrologic regime).

The presence of a gradient as low as that estimated from the WSTP data alone is difficult to account for in light of the hydrologic context and the regional depth to the BSR, however. Well away from the fault outcrop, the BSR lies at a very constant sub-seafloor depth of 95 milliseconds two-way-travel-time (ms TWT) (see Fig. 2), or 80.5 mbsf at a velocity of 1694 m s^{-1} (a velocity determined by com-

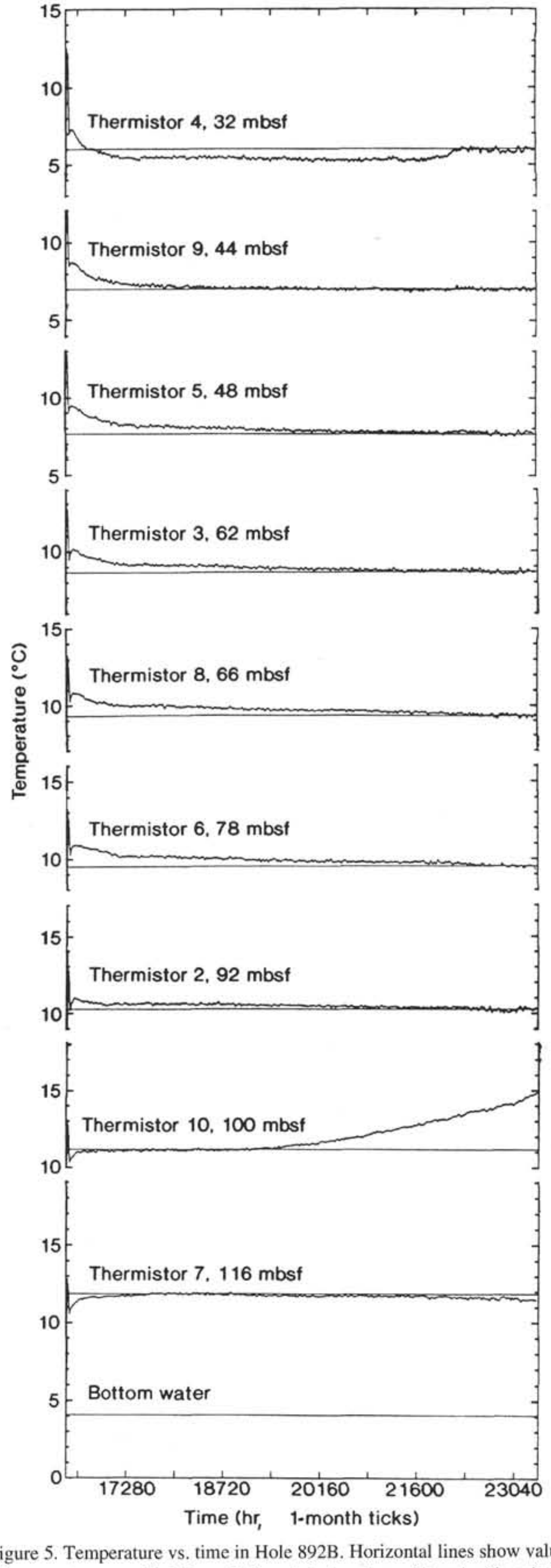

Figure 5. Temperature vs. time in Hole 892B. Horizontal lines show values of temperatures used in Figure 7. Raw data have been filtered with a simple 60-hr running mean to smooth least-significant-bit digital steps. Data for thermistor 1, which was damaged during deployment, are not included. Times in this and other figures are given in hours elapsed since the beginning of 1991, Universal Time Coordinated (UTC). Tick marks are given at roughly 1-month intervals.

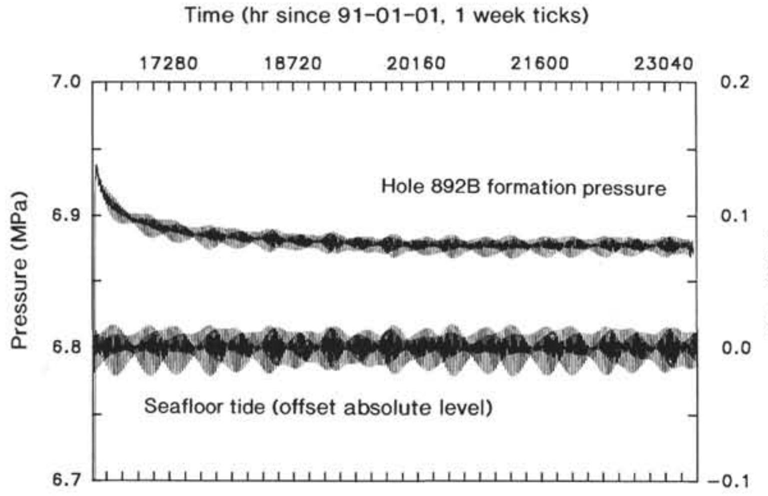

Figure 6. Pressure vs. time in Hole 892B. The estimated seafloor pressure is described in the text.

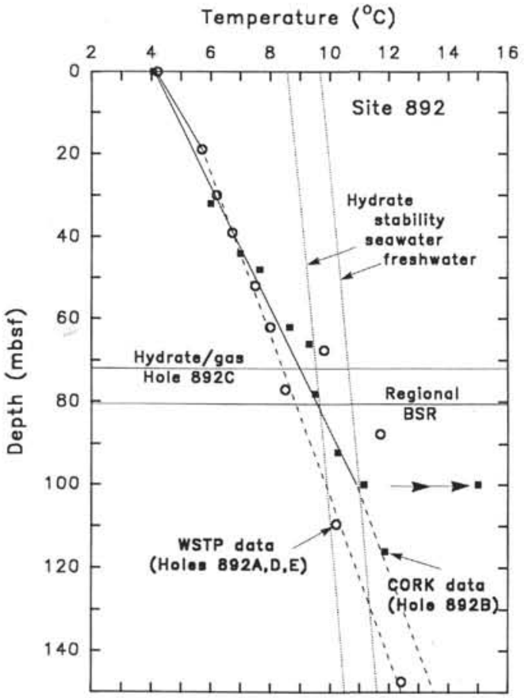

Figure 7. Temperature vs. depth derived from CORK observations (solid squares; see Fig. 5), and from WSTP measurements made during Leg 146 (Shipboard Scientific Party, 1994c; Foucher et al., this volume) (open circles). Shown also are the hydrate stability field P-T boundaries for freshwater- and seawater-methane systems (dotted lines) and depths to the hydrate/gas boundary determined by logging in Hole 892C and to the regional BSR. Solid and dashed lines show the inferred temperature gradients in the hanging wall and footwall of the fault, respectively.

bining the 72-mbsf depth of the sudden decrease in velocity indicated by the velocity log and the two-way travel time to the BSR at the location of Site 892 of 85 ms TWT). Using the depth of 80.5 mbsf, an average thermal conductivity of 1.04 W m^{-1} K^{-1} (Shipboard Scientific Party, 1994c), and the phase relationship for the seawater-methane system (see Fig. 7), a heat flow of 71 mW m^{-2} is inferred. The heat flow determined from the general trend of the CORK data is indistinguishable from this value. Fluid flow up the fault zone will produce locally higher values of heat flow over the hanging wall of the fault (see discussion below), but the value determined from the WSTP data alone is considerably *lower* than the value determined away from the fault. The most reasonable explanation suggested by the model results given below is that the WSTP measurements made deeper than 50–60 mbsf in Holes 892D and 892E were situated below the primary pathway of upward fluid migration, effectively in the footwall of the fault where the thermal gradient is locally diminished (see Fig. 7, dashed lines, and Fig. 11 below). The gradient near the seafloor may be as high as that defined by the seafloor temperature and the first data point, 74 mK m^{-1}, which is indeed elevated relative to the regional value.

Also somewhat enigmatic is the thermal structure of the section relative to the inferred depth of gas-hydrate stability. Reasonable bounds for hydrate stability are provided by the phase relationships of the seawater-methane-hydrate and freshwater-methane-hydrate systems, although the presence of higher hydrocarbons, CO_2, and other constituents can influence the system as well (see discussions in Hyndman and Davis, 1992, and Hyndman et al., 1992). Pressure-temperature relationships summarized by Sloan (1990) and Dickens and Quinby-Hunt (1994) are shown by dotted lines in Figure 7. The average thermal profile defined by the WSTP data (excluding the seafloor datum and the locally anomalous points at 67.5 and 87.5 mbsf) intersects the seawater and freshwater hydrate stability curves at about 100 and 130 mbsf, respectively, well below the depth of the BSR observed anywhere along the seismic reflection profile. The average profile defined by the CORK data intersects the curves at about 82 and 101 mbsf. The greatest depth of hydrate stability in the formation at Site 892 (Hole 892C) appears to be well defined by the velocity-log data, which showed an abrupt transition from relatively high velocities (~1650 m s^{-1}) above 72 mbsf to velocities close to that of seawater (1500 m s^{-1}) below (Shipboard Scientific Party, 1994c). (Any gas present in the sediment would cause formation velocities to be lower than that of water and make the fastest travel path to be through the drilling fluid in the annulus between the logging tool and the hole wall (Shipboard Scientific Party, 1994c). It is possible that some dissociation of hydrate, and thus production of gas in the formation, could have occurred because of the circulation of warm water during drilling (see thermal decays, Fig. 5). However, the abruptness of the velocity transition, and the fact that there would have been sufficient warming to dissociate hydrate at a level well above 72 mbsf (compare early temperatures of thermistor 3, 62 mbsf, in Fig. 5 with Fig. 7), suggests that the boundary is a natural one.) The depth of 72 mbsf is well above any of the depths of stability estimated from the average thermal structure.

To resolve this apparent enigma requires consideration of the anomalous temperatures present in the CORK and WSTP data. Taken point by point, all CORK data fall very close to or above the seawater stability curve below 66 mbsf, as do the WSTP data with the exception of a single point at 77 mbsf. A contemporary fluid flow "event" is suggested below as the cause of the transient thermal anomaly observed in the CORK data at 100 mbsf; it is also reasonable to suggest that a recent event provided the heat to produce a thermal anomaly that may now persist near 72 mbsf and to dissociate previously stable hydrate and create a new elevated hydrate/gas boundary at that depth.

Any more quantitative resolution of this problem is frustrated by the non-coincident location of the holes from which the various data were gathered (Fig. 3). The depth to the abrupt transition in velocity was determined in Hole 892C; WSTP temperatures were measured in Holes 892A, D, and E, and the CORK observations were made in Hole 892B. Lateral variations in heat flow, in the depth-limit of hydrate stability, and in the depth of thermal transients limit the accuracy with which these data can be merged. All of these factors combine to make an accurate determination of the pressure-temperature (P-T) conditions at the point of hydrate stability (and thus a resolution of what the most appropriate phase relationship to use in estimating the temperature at BSR horizons in other similar environments) difficult at this site. However, that the average CORK temperature profile intersects the seawater-hydrate stability limit at the regional depth of the BSR argues strongly that the seawater-methane-hydrate stability curve of Dickens and Quinby-Hunt (1994) can be applied in this accretionary prism setting.

Simulations of the Thermal Effects of Fluid Flow

To investigate the causes of some of the unusual aspects of the thermal structure of Site 892, a finite-element numerical model was used to determine the thermal effects of fluid flow up a fault zone (Figure 8). The thermal structures were calculated both at specific times after the step-wise initiation of flow and at steady state. The hydrologically active part of the fault was simulated as a thin planar horizon. The geometry of the fluid-flow conduit and other aspects of the model were estimated or constrained according to the following observations and assumptions:

1. The fault was assumed to dip to the east at an average of 16°, from the surface outcrop at the bioherm observed by Carson et al. (1994) 350 m northwest of the site, to a depth of 100 m at the location of the holes at Site 892 (Shipboard Scientific Party, 1994c).
2. The thickness of the hydrologically active fault zone was assumed to be less than 2 m as indicated by the scale of organic geochemical anomalies observed in Hole 892A and particularly in Hole 892D.
3. The fluid flow is assumed to have perturbed the near-surface thermal structure in a way defined by the local shoaling of the gas hydrate BSR within a few hundred meters of the fault outcrop, where the inferred heat flow is increased by up to nearly a factor of two (Shipboard Scientific Party, 1994c).
4. The characteristics of a transient fluid flow "event" are constrained by the transient thermal anomaly evident at the level of thermistor 10 situated at 100 mbsf, where the temperature was observed to increase from 11° to 15°C during the last 5.5 months of the recording period. This thermal transient is observed at the level of thermistor 10 only. No change was observed at the adjacent thermistors situated 8 m above and 16 m below.
5. Heat is supplied to the system at great depth conductively at a rate constrained by the depth to the BSR well away from the fault outcrop (see earlier discussion).
6. Latent heat associated with the formation and dissociation of hydrate is ignored.

This is not the only possible model for fluid flow, but it provides the simplest explanation for several of the observations made at Site 892. An alternate possibility is one in which the fault serves as a breach through the near-surface sediments and collects water ascending sub-vertically in the immediate vicinity of the surface trace of the fault. This and other special fluid-flow geometries cannot be precluded, but they are difficult to test with the observational constraints available and thus are not considered here.

Thermal consequences of fluid flow as described by the numerical model are shown in Figures 9–12. The steady-state heat flow at the seafloor above the fault is given in Figure 9 for two rates of fluid flux updip along the planar fault. These results show that there is a critical flux below which no significant thermal perturbation is created and above which large anomalies result. For the fault geometry used, this threshold for steady flux is roughly 2×10^{-7} m^3s^{-1}. (This and other fluid-flux values quoted in the text and figures are given as volumetric rates per-meter-strike-length of the fault. Darcian velocities can be obtained by dividing the volumetric fluxes by the thickness of the hydraulically active fault zone). The results also show that when the fluid flux is sufficient to produce a significant thermal anomaly near the fault outcrop, a significant difference in the heat flow between the footwall and hanging wall also develops far from the outcrop. This consequence is well known and approximately described by the relationship

$$q(\text{hanging wall}) - q(\text{footwall}) = f\rho\ C\ dT/dz\ \sin(\theta),$$

where f is the volumetric fluid flux, ρ is the fluid density, C is the heat capacity per unit mass of the fluid, and θ is the dip of the fault

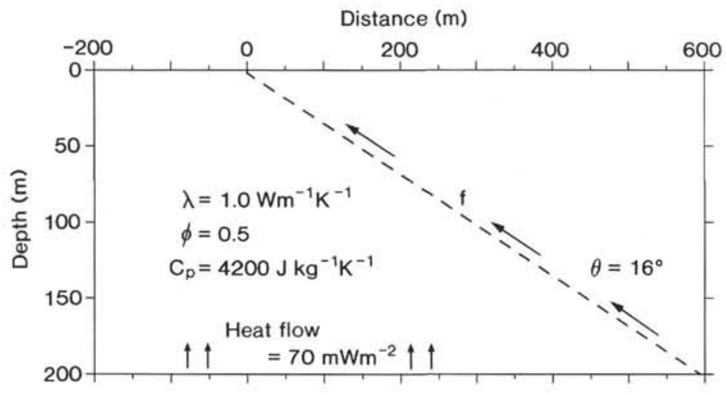

Figure 8. Geometry and physical properties used in finite-element thermal simulation of fluid flow up a thin fault beneath ODP Site 892. Heat flow is supplied conductively to the footwall. Physical properties are uniform throughout the model.

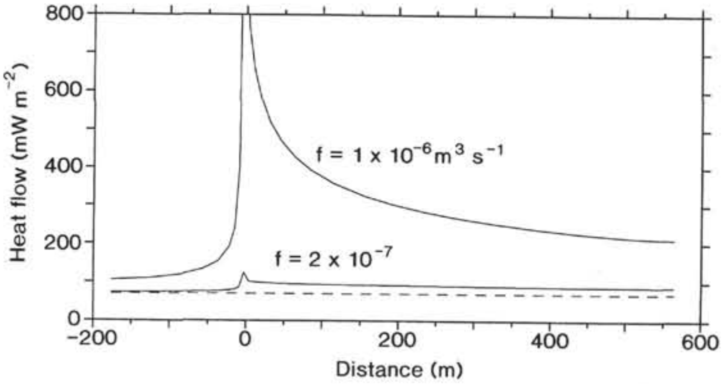

Figure 9. Steady-state seafloor heat flow calculated using the model described in Figure 8 for two rates of fluid flow (*f*). The rates shown (given here and in Figs. 10–12 as volumetric fluxes per meter strike-length of fault) bound the "threshold" rate above which the associated thermal perturbation is geothermally significant.

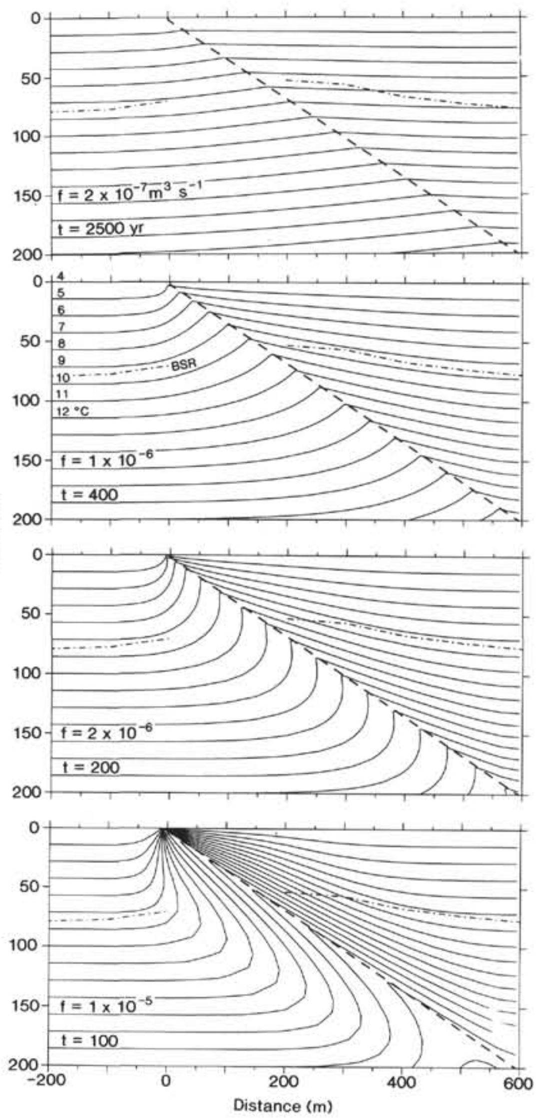

Figure 10. Thermal structure calculated using the model described in Figure 8 for four rates of fluid flow. Isotherms are given in 1-K increments and are compared to the thermal structure inferred from the depth to the gas-hydrate bottom simulating reflector (BSR) in the vicinity of Site 892 (dashed line; see Fig. 2). Results are shown for times after the onset of flow (*t*) when the best match to the BSR thermal structure was achieved. An acceptable match was never achieved with flow rates less than 4×10^{-7} m^3s^{-1} or greater than 4×10^{-6} m^3s^{-1}.

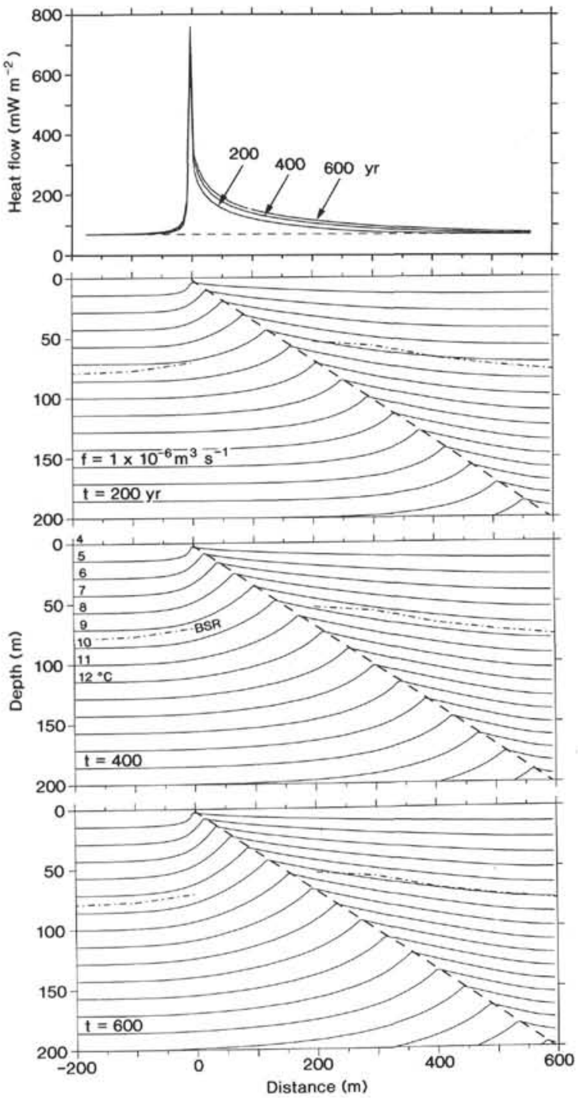

Figure 11. Seafloor heat flow and thermal structure calculated using the model described in Figure 8 for the optimum flow rate (1×10^{-6} m^3s^{-1}; see Fig. 10) at three times after the initiation of fluid flow.

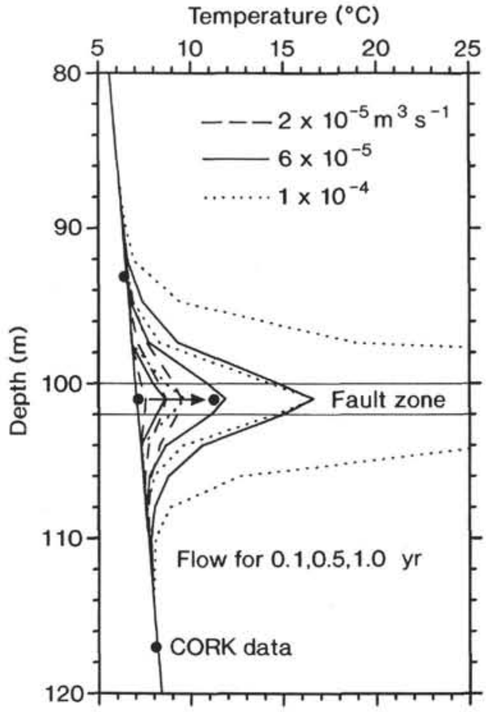

Figure 12. Temperature-depth profile calculated using the model described in Figure 8 soon after step-wise initiation of fluid flow. Profiles are shown for three different rates of flow, and at 0.1, 0.5, and 1.0 yr after the initiation of flow. The model results are compared to CORK data points, including that from thermistor 10, which increased over the last 5.5 months of recording. The coincidence of the fault zone and thermistor 10 is assumed.

(Lewis and Beck, 1977). That the heat flow, *q*, inferred from the depth to the BSR, is identical on the hanging wall and footwall blocks a few hundred meters from the fault outcrop implies that the hydrologic system at Site 892 has not reached steady state.

A variety of transient thermal states are explored in Figures 10 and 11. These results show that the thermal anomaly defined by the shoaling of the BSR can be accounted for by transient flow, and that both the rate and history of flow can be reasonably well constrained.

Sensitivity to the rate of flow is demonstrated in Figure 10, where the level of the BSR is compared to the cross-sectional thermal structure in the vicinity of the fault. Simulations were reviewed at several time steps in order to choose the "optimum" history of flow at each flow rate. This choice was based on how well the local anomaly near the fault outcrop could be matched while not causing the thermal structure at the level of the BSR several hundred meters away from the fault to be perturbed. The thermal structure inferred from the depth of the BSR is best matched by flow up the fault at a rate of 1×10^{-6} m^{3}s^{-1} that initiated 400 years ago (Fig. 10). Thermal structures at times on either side of this optimum solution are shown in Figure 11 to illustrate the sensitivity to the history of flow. Both the rate of flow and the initiation time appear to be determined to within a factor of two. In the optimal case, the modeled thermal structure matches the "isotherm" defined by the position of the BSR to within 0.5°C.

Two other predictions of the model are useful in providing additional tests of the validity of the model, and constraints on the nature of the fault zone and on the rate and history of fluid flow. These are: (1) the seafloor heat flow, which is largest in the near-vicinity of the fault outcrop, and, in transient cases, differs from the heat flow that would be predicted from the depth of the BSR at intermediate distances from the fault outcrop (Fig. 11); and (2) the heat flow at depth, which changes abruptly across the fault (Figs. 10 and 11). Unfortunately, there are no clear observational constraints that can be compared to these predictions of the model. No seafloor heat flow measurements have been made in the vicinity of this fault, and only one temperature determination was made unequivocally below the fault. As discussed earlier, however, if the seafloor temperature is ignored, the WSTP measurements in general define an enigmatically low gradient. It is possible that at the location where the measurements were made (low-temperature points deeper than 50 mbsf were made in Hole 892D, which is located farthest west and closest to the fault outcrop) the deeper measurements were in fact made at levels *below* the currently hydrologically active fault. The higher gradient between the seafloor and the shallowest sediment temperature points may define the thermal structure of the hanging-wall block.

If fluid flow is sufficiently fast, thermal inversions (positive temperature anomalies bounded below by a negative temperature-depth gradient) can develop at early times (Fisher and Hounslow, 1990). This is evident in one case shown in Figure 10, where the thermal structure produced after 100 years of fluid flow at 1×10^{-5} m^{3}s^{-1} is shown. While an inversion of this magnitude and scale is not evident in any of the data, smaller local inversions are indicated by both the WSTP and CORK data (Shipboard Scientific Party, 1994c; Fig. 7). It was speculated that these anomalies were the result of recent fluid-flow "events," as were local thermogenic hydrocarbon anomalies (Shipboard Scientific Party, 1994c; see discussion above). The best example of a fluid-flow event may have been captured in progress at the level of thermistor 10 as described above (see Figures 5 and 7).

To estimate the quantitative nature of the fluid-flow event that may have caused this thermal anomaly, the numerical model described above was again employed. Results presented in Figure 12 show the temperature-depth structure in the immediate vicinity of the dipping fluid conduit for three rates of fluid flux and at three times after the onset of flow. The depth interval within which the anomaly was confined in the course of 5.5 months of observation crudely constrains the position of the fracture or fracture zone that hosted the flow. No anomaly is observed at the thermistors 8 m above or 16 m below thermistor 10. The rate of flow is constrained by the amplitude of the event. A lower limit of 6×10^{-5} m^{3}s^{-1} is established by assuming that thermistor 10 and the fracture were co-located. The thermal anomaly produced by a slightly higher rate of flow would match the observational constraints if the fault were a few meters deeper, but the ranges of possible flow rates and fault positions are not large. The lower limit of flow rate is nearly two orders of magnitude higher than the longer-term average rate inferred from the perturbation of the depth to the BSR, suggesting that these transient events must be relatively infrequent. If the fault zone were 1 m thick, the Darcian velocity and the duration of the event would suggest that the fluid in the fault zone at the end of the 5.5-month period of observation were derived from a depth of 360 mbsf, where the formation temperature is of the order of 30°C. This temperature is insufficient to produce the thermogenic hydrocarbons observed in the discrete zones in Holes 892A and C; a much greater source depth is required. This implies either that pulses like this one must persist for longer periods of time, that batches of fluid from deep in the section must be brought progressively higher by temporally isolated events, or that the pulses are superimposed on a deep-source background flow that is too slow to be detected thermally.

The primary implications of the results of these simple models that successfully describe the sub-seafloor thermal structure in the vicinity of Site 892 are that (1) thermally significant rates of fluid flow up the fault zone at this location can have persisted for only a few hundred years, and (2) the average rate of flow (over the past few hundred years) may comprise numerous short-lived pulses of fluid flow, each being perhaps two orders of magnitude more rapid than the average flow.

FORMATION PRESSURE

Equilibrium Pressure

The long-term decay of pressure with the tidal component removed by filtering is shown in Figure 13. At the time the CORK was initially sealed in, the pressure in the hole is seen to have climbed to a maximum of 6938 kPa, approximately 70 kPa above hydrostatic pressure determined prior to shut-in (and confirmed during the second recording period in which the hole was left open). Pressure then began falling toward hydrostatic conditions (as defined by seawater density at the formation geotherm) over the next 5 months. There was a slight tendency for pressure to increase over the final 4 months of recording, but the change was very small, about 2 kPa. Final pressure in the hole was fairly steady at just 13 kPa above hydrostatic.

The first ten days of the pressure decay recorded by the CORK is placed in context of earlier observations of pressure made at the time of shipboard packer experiments in Figure 14. The level of background pressure to which slug- and post-injection transients dissipated was roughly 250 kPa (superhydrostatic), and there appears to have been a tendency for the background pressure to decrease during the four-hour period of testing (Shipboard Scientific Party, 1994c, fig 73; Screaton et al., this volume). During some of the pump tests, super-lithostatic pressures (630 kPa above hydrostatic at 100 mbsf at an average grain density of 2600 kg m^3 and average porosity of 0.6; Shipboard Scientific Party, 1992c) are known to have been reached, and clear signs of hydrofracturing were seen at a pressure well below the lithostatic level (Shipboard Scientific Party, 1994c; Screaton et al., this volume). The pressure required to maintain open fractures during three constant-rate injection tests was as low as 450 kPa above hydrostatic (Shipboard Scientific Party, 1994c, fig. 73), about 180 kPa less than lithostatic at 100 mbsf. The pressure at the point of fracture closure was inferred from injection recovery curves to be even less than this (~320 kPa; Screaton et al., this volume). In Figure 14 it is assumed that this level of pressure was reached during drilling and cementing operations, although no good constraints on how much backpressure can develop in the annulus outside the drill string during circulation are available. A steady decay is crudely defined in this plot, from the possible initial pressure of between 320 and 450 kPa (relative to hydrostatic) at the time of final drilling activity, through roughly 200-250 kPa at the time of the packer work, to 70 kPa at the time of CORK shut-in, and ultimately to 13 kPa 5 months later.

Three ways to account for the initial formation pressure transient are considered here. The second two are also discussed by Screaton et al. (unpubl. data). The first involves the thermal perturbation caused by drilling, which in some cases can create a large anomalous pressure. This is caused by the density difference between the undisturbed formation fluid and the fluid that has been circulated in the hole at the time of drilling, and it can last for several months. In the extreme case of Hole 857D, drilled to 936 mbsf in the Middle Valley rift of the Juan de Fuca Ridge, the integrated difference between the hot formation and the initially cold column of water in the hole created a pressure anomaly of over 1 MPa (Davis and Becker, 1994). In that case, the initial pressure in the sealed hole was sub-hydrostatic. To create anomalous hole pressures that are super-hydrostatic, the water in the hole must be warmer on average than the water in the surrounding formation. This may have been the case in Hole 892B, although initial conditions over the full depth of the hole are not well defined. Above 100 mbsf, shut-in temperatures were typically about 2 K warmer than final formation temperatures (Fig. 5). Deeper than 100 mbsf, initial hole temperatures were probably cooler than the formation, and thus the integrated thermally-induced pressure anomaly may have been either positive or negative. Regardless of the sign, the amplitude of the pressure anomaly associated with a 2-K temperature difference is far to small to account for the observed pressure transient. Integrated over a depth of 100 m, a 2-K temperature difference results in only a 0.4 kPa pressure anomaly, and thus this explanation for the cause of the pressure transient is precluded.

A second explanation for the long-term pressure variation in Hole 892B is that the undisturbed formation pressure was large and super-hydrostatic, and that a slow leak in the CORKed hole (such as one from the hole to the seafloor via ineffective grout between the casing and the formation or via a pilot hole, or one from an isolated over-pressured zone to the rest of the formation spanned by the perforated casing) allowed this pressure to drain down to close to a hydrostatic level. Any leak in the annulus outside the casing would have to be sufficiently resistive to damp the relatively high-frequency seafloor tidal pressure variations signal (see discussion below), but sufficient-

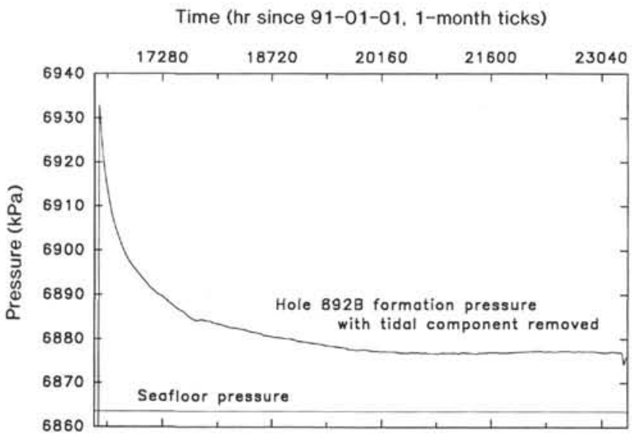

Figure 13. Long-period pressure variation in Hole 892B, with the tidal component removed. Tickmarks are given at approximately 1-month intervals.

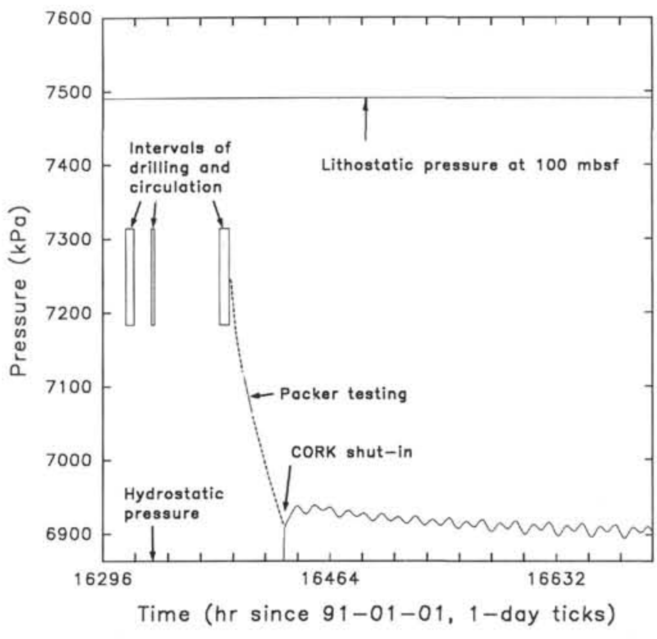

Figure 14. Speculated history of pre-CORK shut-in pressure in Hole 892B, along with the early part of the post-shut-in pressure record. The vertical axis origin has been adjusted to hydrostatic. Boxes show speculated pressures at times during which drillwater, mud, or cement was circulated in the hole. The solid line segment shows the level and approximate trend of background pressures present during packer tests. Minor tick marks are given at 1-day intervals.

ly transmissive to allow drainage over the four-month period observed in Figure 13. That the pressure reached a low, but relatively stable superhydrostatic value argues that, if this explanation is correct, the "leak" must have been from a relatively low-capacity, but highly permeable, over-pressured zone into the surrounding formation characterized by high-capacity, low-permeability, and low overpressure. Leakage to the seafloor from a generally high-pressure formation would have resulted in continuing decay towards hydrostatic pressure.

A third possibility is that the formation was charged with water during drilling and the long-term variation seen in Figure 13 is simply the natural transient decay from that artificial perturbation.Unfortunately, there are few constraints on what the degree of charging might have been, although there is little question that pressures equal to or exceeding that shown in Figure 14 could have been reached at various stages during drilling, flushing, and cementing. If high pressures persisted for any length of time, hydrofracturing could have assisted in allowing a large volume of the formation surrounding the hole to be affected because of the temporarily enhanced permeability. The long time-constant associated with the decay may simply reflect the large volume of the formation affected by charging, and the low permeability of the formation that was reestablished after the initially high pressures had dissipated and fractures had closed.

Determining which of the latter two explanations is correct is clearly important; if leakage is present, then the formation pressure within the fault zone could be as high as 450 kPa above hydrostatic (0.65 times lithostatic); if not, then the pressure in the zone must only be of the order of 13 kPa (less than 0.02 times lithostatic). An unequivocal distinction between these possibilities cannot be made with the data in hand, although Screaton et al. (unpublished data) favor the former on the basis of the pressure-dependence of their transmissivity determinations and a simple order of magnitude calculation: to transmit fluid along the fault zone at a rate sufficient to perturb the BSR, the fault zone transmissivity is constrained to be as high as values determined during injection tests, when fractures were opened by high fluid pressure.

This conclusion is consistent with the results presented here: requirements for fault zone transmissivity can be calculated by assuming that flow is driven on average at a rate of 1×10^{-6} m s^{-1} (the "background" rate of flow required to deflect the BSR; Figs. 10 and 11), and locally at a rate of 6×10^{-5} m s^{-1} (the rate inferred from the thermal transient at 100 mbsf; Fig. 12), by a pressure gradient of the order of 1 kPa m^{-1} (i.e., assuming that the limiting pressure for hydrofracture of 450 kPa is available to drive fluid along the length of the fault to the seafloor). A 1-m-thick fault zone is assumed in the calculations. The results are summarized in Figure 15, where transmissivities from these calculations are compared to those determined by Screaton et al. (this volume) and from the phase of the CORK tidal signal (see discussion below). Clearly, the transmissivity required to permit flow at either the average or transient rate is far larger than the values determined from the *Alvin* pumping tests and the CORK tidal data after formation pressures had dissipated. Transmissivities determined at pressures near the limit for hydrofracturing by Screaton et al. (this volume) are clearly required, and thus we conclude as do Screaton et al. (this volume), that the natural pressures in the fault zone must be maintained at a level sufficient to maintain open fractures, of the order of 300 to 450 kPa, or roughly 0.45 to 0.65 times lithostatic.

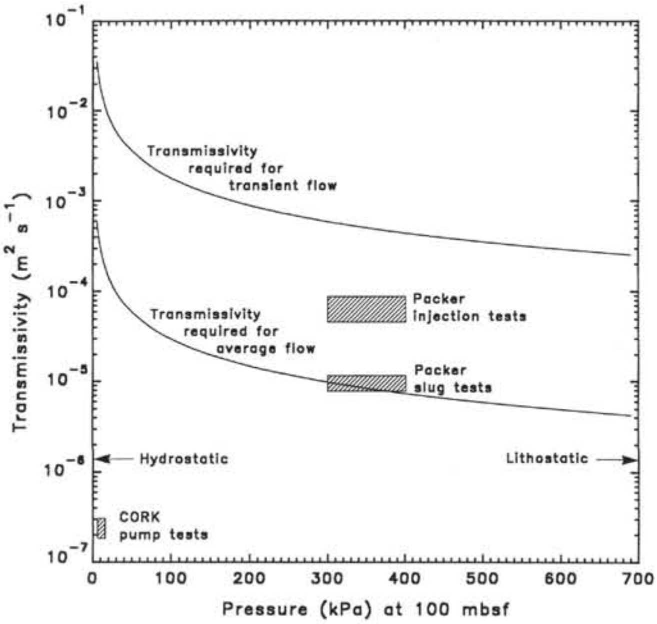

Figure 15. Transmissivity required for flow in a 1-m-thick fault zone at rates estimated for transient and average fluid flow (Figs. 11 and 12) as a function of driving pressure. The flow geometry indicated in Fig. 8 is assumed. Also shown are transmissivities estimated by Screaton et al. (this volume) from shipboard packer and CORK pumping experiments, which are clearly sensitive to formation pressure.

Tidal Loading Phase and Attenuation

The tidal component of the formation pressure signal in Hole 892B is shown in Figure 16, along with the tidal signal estimated using astronomical harmonic components with a local calibration with long-term seafloor pressure gauge recordings at Cobb Seamount. A phase shift equivalent to 0.4 hours has been applied to the Cobb tidal function to account for the phase difference between the reference tidal station and Site 892 (M. Foreman, pers. comm., 1994). The accuracy with which this predictive function can be applied to Site 892 is indicated in Figure 16A, where the 0.4-hr-shifted predicted tidal signal is compared to the CORK data recorded during the second year of monitoring, when the fluid sampling port was left open. The agreement is excellent.

During the first year of monitoring, when the sampling port was closed, the formation tidal signal was attenuated by a factor of 0.5, and advanced by 0.3 hr relative to the local seafloor tidal pressure (0.7 hr relative to the Cobb reference signal). The attenuation and phase are seen to be consistent throughout the recording period (cf. Fig. 16B and 16C).

A one-dimensional elastic model for tidal loading allows the bulk modulus and a limit on the permeability of the section in the vicinity of the perforated casing to be estimated from the characteristics of the tidal signal propagation (Van der Kamp and Gale, 1983; K. Wang and E. Davis, unpubl. data). The attenuation is sensitive to the ratio of the sediment frame (drained) modulus and the modulus of the fluid filling the sediment pore volume. Using a value for the pore-water modulus at the appropriate temperature and pressure (2.2×10^9 Pa) and a frame Poisson's ratio of 0.1, the unconfined frame modulus is calculated to be 1.9×10^9 Pa. This value is roughly a factor of fifty greater than that determined by Hamilton (1971) for sediment of an average porosity of 50% (a value appropriate for the section at roughly 100 mbsf; Shipboard Scientific Party, 1994c) (Fig. 17).

Two explanations, or a combination thereof, for this disparity are possible. One is that the sediment is anomalously rigid for its porosity (equivalent to sediment of less than 30% porosity) because of the de-

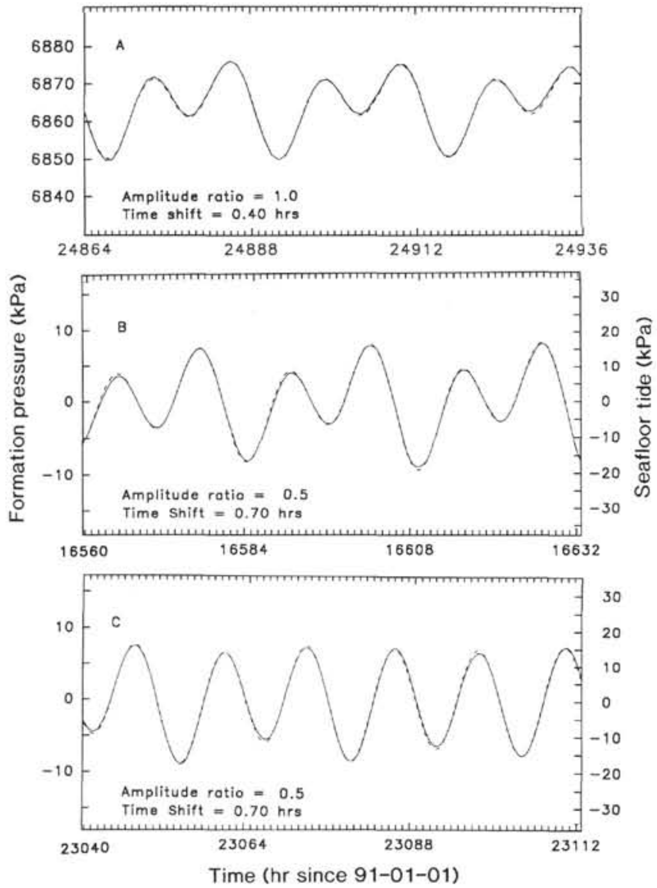

Figure 16. Estimated seafloor (dashed lines; see text) and CORK formation tidal pressure variations (solid lines) at Site 892. Records are shown at (**A**) a time when the CORK seal was bypassed by the fluid sampling port, allowing local calibration of the predicted seafloor tidal function, and at (**B**) early and (**C**) late parts of the monitoring period when the fluid sampling port was closed. Amplitudes have been adjusted and times shifted to show the attenuation factor and phase of the formation signal relative to the seafloor tide.

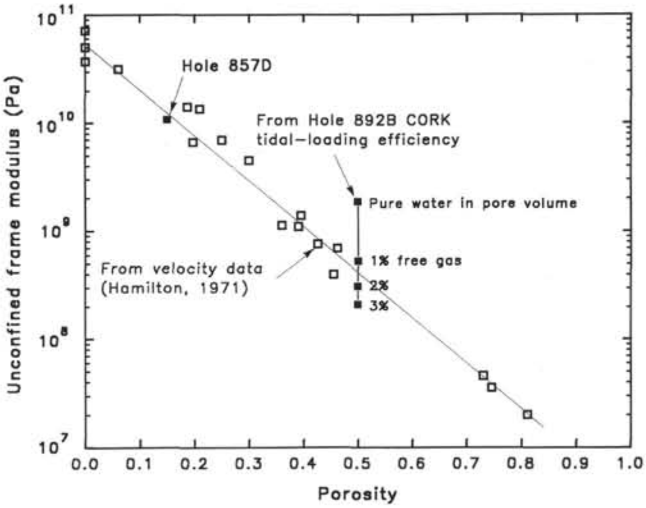

Figure 17. Unconfined frame (drained) bulk modulus calculated from the seafloor tidal pressure signal attenuation in Holes 857D (Davis and Becker, 1994; K. Wang and E. Davis, unpublished data) and 892B compared to values determined for marine turbidite sediments by Hamilton (1971). Effects of free gas in Hole 892B, to which tidal attenuation is highly sensitive, are shown.

gree of deformation and cementation it has experienced. The second is that the pore fluid contains a significant quantity of free gas. The effect of various amounts of methane (% by volume, with a modulus of 8.6×10^6 Pa) is shown in Figure 17. To account for the discrepancy by this factor alone would require the pore volume to contain between 1% and 2% free gas. Free gas was inferred to be present from the level of the BSR to the bottom of Hole 892C on the basis of velocity logging results (Shipboard Scientific Party, 1994c), and free gas may have been the cause of the high system compressibility observed during packer testing (Screaton et al., this volume). The amount of gas was not well constrained by those data, however; the estimate derived here from the tidal signal attenuation probably provides the best constraint on the amount of gas in the section.

Another characteristic of the formation tidal signal, specifically the 0.3 hr phase lead, also suggests the presence of gas, and provides a constraint on permeability (Van der Kamp and Gale, 1983; E. Davis and K. Wang, unpubl. data). That the formation signal leads the tidal loading signal suggests that the interval of open hole is situated beneath, not within, a gas-bearing interval. The large magnitude of the leading phase requires a high-permeability connection between the interval of perforated casing and the gas-bearing interval above (Davis and Wang, unpubl. data). This is most easily attributed to the fault zone. The possibility that a quantity of free gas had collected in the hole itself can be excluded, as this would cause a very large degree of signal attenuation and a lag in phase.

SUMMARY

Nine and one-half months of CORK observations in the hydrologically sealed Hole 892B in the Cascadia accretionary prism provide new constraints on the thermal structure of the hydrologically active fault zone intersected by this hole, about the formation pressure, and about the average mechanical and hydrologic properties of the sediment section in the interval spanned by the section of screened casing below 94 mbsf. Primary conclusions and inferences drawn from the observations are summarized as follows:

1. Temperatures define a generally uniform gradient = 68 mK m^{-1} (heat flow = 71 mW m^{-2}) that is significantly greater than that defined by WSTP measurements made at the time of drilling. This disagreement can be accounted for if most of the WSTP measurements were made below zones of fluid upflow. This is generally consistent with the position of the holes with respect to the fault outcrop: the CORKed hole is farther from the outcrop than any of the exploratory holes in which the WSTP measurements were made, and thus the latter may penetrate a lesser amount of the hanging-wall section.
2. As was observed in the WSTP data, temperatures at a few isolated levels lie well above the "background" trend. In two cases true thermal inversions are defined; these require a transient source of heat. At the 100 mbsf level of CORK thermistor 10, a transient event was detected. It is likely that the thermal anomalies occurred at depths where sediments were locally fractured and of higher porosity (as indicated by logging and physical properties in Holes 892A, C, D, and E), and where fluid flow was indicated by the occurrence of thermogenic hydrocarbons (Holes 892A and D). The limited depth extent of the chemical anomalies limits the thickness of hydrologically

active intervals. In Hole 892D a transition from background to high hydrocarbon concentrations occurs in less than one meter, although in most instances, sampling intervals preclude determining the extent of the anomalies to better than a few meters. The limited extent of the thermal anomalies (less than ± 10 m) limits both the thickness of the hydrologically active intervals and the time over which flow can have been active. The amplitude of the transient thermal anomaly (rising by 4 K in 5.5 months) constrains the volumetric flow rate to be at least 6×10^{-5} m^3s^{-1} (flux per m strike-length of the fault; equivalent to a Darcian velocity of 6×10^{-5} ms^{-1} for a fault zone 1 m thick). The average rate of fluid flow required to produce a local seafloor heat-flow anomaly, as indicated by the elevated BSR at the fault, is only 1×10^{-6} m^3s^{-1}, much lower than the rate estimated for the local transient event. The average flow thus may be the sum of numerous and rapid, but localized and short-lived, transient flow events.
3. To host flow at a rate as high as 6×10^{-5} m^3s^{-1}, the fault zone must be exceptionally transmissive. At a pressure gradient estimated by Screaton et al. (this volume) of roughly 0.5 times lithostatic, the transmissivity must be locally as high as 4×10^{-4} m^2s^{-1} to support the high inferred rate of transient fluid flow. To create this level of transmissivity probably requires high fluid pressures which, like fluid flow, probably occur episodically.
4. On a longer time scale, the "average" fluid flow at Site 892 also appears to be transient. This conclusion is required by the observation that the heat flow anomaly near the fault outcrop indicated by the locally shallow BSR is not accompanied by a regional change in heat flow between the hanging wall and footwall of the fault that would be present if fluid flow up the fault were steady. Results of numerical models suggest that the flow that has produced the current thermal regime has persisted for only a few hundred years. It is tempting to speculate that this fluid-flow transient may be tied to the 300–600-yr-period Cascadia subduction zone megathrust cycle (Adams, 1990).
5. The spatial separation of the holes over the dipping fault zone at Site 892 and the consequent lack of co-located observations, along with the local transient thermal structure of the section, frustrate efforts to use the temperature data together with the depth to the level of gas-hydrate stability as a P-T calibration point for the methane-water-hydrate system. Despite the complications, however, the CORK data may provide one of the best observational constraints on the P-T conditions at a BSR. The average temperature profile defined by the CORK data (with the exclusion of points where the effect of fluid flow is suspected) intersects the seawater-methane-hydrate P-T stability profile at a depth that is indistinguishable from the regional depth to the BSR. Near the locally anomalous BSR depth, no measured temperatures in the holes fall close to that required for freshwater-hydrate dissociation.
6. Pressure in the borehole rose immediately to a value about 70 kPa above hydrostatic at the time of shut-in, then decayed over the following five months to a steady formation value 13 kPa above hydrostatic. The initially superhydrostatic value may have been caused by the charging of the formation at the time of drilling. It is more likely, however, that the decay resulted from dissipation of naturally high fluid pressures in the fault zone to the surrounding formation via the connection made by the open section of borehole, or possibly to the seafloor via leakage through ineffective cement around the solid casing.
7. Observed attenuation of the seafloor tidal loading signal by the formation (a factor of 0.5) constrains the unconfined frame modulus of the sediment section to be 1.9×10^9 Pa if the pore volume of the sediment is filled with seawater. This estimate is roughly fifty times higher than values determined by Hamilton (1971) for terrigenous marine sediments having a porosity of 50% (the average over the interval of perforated casing). Accounting for 1–2% free gas in the sediment brings the values into agreement at 4×10^8 Pa.
8. The seafloor tidal loading signal was observed to lead the formation by 0.3 hours. This observation can be explained by the presence of free gas in the section above the interval of perforated casing and below the BSR and by a highly permeable zone connecting the interval bearing free gas and the interval of open hole.

ACKNOWLEDGMENTS

The authors gratefully acknowledge the exceptional talents and invaluable contributions of Bob Macdonald and Tom Pettigrew for CORK engineering development and shipboard deployment and of Bob Meldrum for instrument construction and calibration. The very robust data loggers were built by Richard Branker Research, Ltd., and the thermistor cables by Cortland Cable Company, Inc. Thanks are also extended to the captain and crew of the ODP drilling vessel *Sedco BP 471* for their assistance with the CORK deployments, to the captain and crew of the *Atlantis II,* and to *Alvin* pilots Bob Grieve, Pat Hickey, and Dudley Foster for their assistance with data recovery operations. Elizabeth Screaton kindly provided unpublished results of *Alvin* pumping tests. Financial support was generously provided by the Ocean Drilling Program, the Geological Survey of Canada, and the National Science Foundation through grants OCE-9012344 and OCE-9301995. GSC Contribution Number 52094.

REFERENCES

Adams, J., 1990. Paleoseismicity of the Cascadia subduction zone: evidence from turbidites off the Oregon-Washington margin. *Tectonics,* 9:569–583.

Carson, B., Seke, E., Paskevich, V., and Holmes, M.L., 1994. Fluid expulsion sites on the Cascadia accretionary prism: mapping diagenetic deposits with processed GLORIA imagery. *J. Geophys. Res.,* 99:11954–11969.

Cochrane, G.R., MacKay, M.E., Moore, G.F., and Moore, J.C., 1994. Consolidation and deformation of sediments at the toe of the central Oregon accretionary prism from multichannel seismic data. *In* Westbrook, G.K., Carson, B., Musgrave, R.J., et al., *Proc. ODP, Init. Repts.,* 146 (Pt. 1): College Station, TX (Ocean Drilling Program), 421–426.

Davis, E.E., and Becker, K., 1994. Formation temperatures and pressures in a sedimented rift hydrothermal system: ten months of CORK observations, Holes 857D and 858G. *In* Mottl, M.J., Davis, E.E., Fisher, A.T., and Slack, J.F. (Eds.), *Proc. ODP, Sci. Results,* 139: College Station, TX (Ocean Drilling Program), 649–666.

Davis, E.E., Becker, K., Pettigrew, T., Carson, B., and MacDonald, R., 1992. CORK: A hydrologic seal and downhole observatory for deep-ocean boreholes. *In* Davis, E.E., Mottl, M.J., Fisher, A.T., et al., *Proc. ODP, Init. Repts.,* 139: College Station, TX (Ocean Drilling Program), 43–53.

Dickens, G.R., and Quinby-Hunt, M.S., 1994. Methane hydrate stability in seawater. *Geophys. Res. Lett.,* 21:2115–2118.

Fisher, A.T., and Hounslow, M.W., 1990. Transient fluid flow through the toe of the Barbados accretionary complex: constraints from Ocean Drilling Program Leg 110 heat flow studies and simple models. *J. Geophys. Res.,* 95:8845–8858.

Hamilton, E.L., 1971. Elastic properties of marine sediments. *J. Geophys. Res.,* 76:579–604.

Hyndman, R.D., and Davis, E.E., 1992. A mechanism for the formation of methane hydrate and seafloor bottom-simulating reflectors by vertical fluid expulsion. *J. Geophys. Res.,* 97:7025–7041.

Hyndman, R.D., Foucher, J.P., Yamano, M., Fisher, A., Berner, U., Brückmann, W., Byrne, T., Chabernaud, T., Firth, J.V., Gamo, T., Gieskes, J.M., Hill, I.A., Karig, D.E., Kastner, M., Kato, Y., Lallemand, S., Lau, R., Maltman, A.J., Moore, G.F., Moran, K., Olafsson, G., Owens, W.H., Pickering, K., Siena, F., Taira, A., Taylor, E., Underwood, M.B., Wilkinson, C., and Zhang, J., 1992. Deep sea bottom-simulating-reflectors: calibration of the base of the hydrate stability field as used for heat flow estimates. *Earth Planet. Sci. Lett.,* 109:289–301.

Lewis, T.J., and Beck, A.E., 1977. Analysis of heat-flow data: detailed observations in many holes in a small area. *Tectonophysics,* 41:41–59.

Linke, P., Suess, E., Torres, M., Martens, V., Rugh, W.D., Ziebis, W., and Kulm, L.D., 1994. In situ measurement of fluid flow from cold seeps at active continental margins. *Deep Sea Res.,* 41:721–739.

Screaton, E.J., and Carson, B., 1993. Results from ODP Leg 146 sealed boreholes: shipboard and submersible-based hydraulic tests. *Eos,* 74:578.

Shipboard Scientific Party, 1994a. Leg 146 introduction: Cascadia Margin. *In* Westbrook, G.K.,Carson, B., Musgrave, R.J., et al., *Proc. ODP, Init. Repts.,* 146 (Pt. 1): College Station, TX (Ocean Drilling Program), 5–14.

————, 1994b. Sites 889 and 890. *In* Westbrook, G.K., Carson, B., Musgrave, R.J., et al., *Proc. ODP, Init. Repts.,* 146 (Pt. 1): College Station, TX (Ocean Drilling Program), 127–239.

————, 1994c. Site 892. *In* Westbrook, G.K., Carson, B., Musgrave, R.J., et al., *Proc. ODP, Init. Repts.,* 146 (Pt. 1): College Station, TX (Ocean Drilling Program), 301–378.

Sloan, E.D., 1990. *Clathrate Hydrates of Natural Gasses:* New York (Marcel Dekker).

Van Der Kamp, G., and Gale, J.E., 1983. Theory of earth tide and barometric effects in porous formations with compressible grains. *Water Resour. J.,* 19:538–544.

Date of initial receipt: 6 September 1994
Date of acceptance: 23 February 1995
Ms 146SR-219